

Diverse Impacts of the Indian Ocean Dipole on El Niño–Southern Oscillation[©]

LEI ZHANG,^a WEIQING HAN,^a GERALD A. MEEHL,^b AIXUE HU,^b NAN ROSENBOOM,^b TOSHIAKI SHINODA,^c AND MICHAEL J. MCPHADEN^d

^a Department of Atmospheric and Oceanic Sciences, University of Colorado Boulder, Boulder, Colorado

^b National Center for Atmospheric Research, Boulder, Colorado

^c Department of Physical and Environmental Sciences, Texas A&M University–Corpus Christi, Corpus Christi, Texas

^d NOAA/Pacific Marine Environmental Laboratory, Seattle, Washington

(Manuscript received 27 January 2021, in final form 17 August 2021)

ABSTRACT: Understanding the impact of the Indian Ocean dipole (IOD) on El Niño–Southern Oscillation (ENSO) is important for climate prediction. By analyzing observational data and performing Indian and Pacific Ocean pacemaker experiments using a state-of-the-art climate model, we find that a positive IOD (pIOD) can favor both cold and warm sea surface temperature anomalies (SSTA) in the tropical Pacific, in contrast to the previously identified pIOD–El Niño connection. The diverse impacts of the pIOD on ENSO are related to SSTA in the Seychelles–Chagos thermocline ridge (SCTR; 60°–85°E, 7°–15°S) as part of the warm pole of the pIOD. Specifically, a pIOD with SCTR warming can cause warm SSTA in the southeastern Indian Ocean, which induces La Niña–like conditions in the tropical Pacific through interbasin interaction processes associated with a recently identified climate phenomenon dubbed the “warm pool dipole.” This study identifies a new pIOD–ENSO relationship and examines the associated mechanisms.

KEYWORDS: Pacific Ocean; Indian Ocean; ENSO; Climate variability

1. Introduction

El Niño–Southern Oscillation (ENSO) is the dominant mode of interannual climate variability on the planet (McPhaden et al. 2006) (Fig. 1a). It is associated with substantial changes in the ocean–atmosphere coupled system in the tropical Pacific Ocean (Bjerknes 1969). Through the atmospheric bridge, ENSO has prominent climatic impacts around the globe (Wallace and Gutzler 1981). For instance, it has been well recognized that El Niño/La Niña can induce basinwide positive/negative sea surface temperature anomalies (SSTA) in the tropical Indian Ocean (Alexander et al. 2002; Klein et al. 1999). On the other hand, the tropical Indian Ocean also exhibits strong interannual climate variability manifested as an east–west dipole-like SSTA pattern, referred to as the Indian Ocean dipole (IOD) (Saji et al. 1999; Webster et al. 1999) (Fig. 1b). While the basinwide warming/cooling pattern of Indian Ocean SSTA is primarily forced by ENSO, the IOD can exist independently of ENSO (Behera et al. 2006; Yang et al. 2015). Like ENSO, the IOD also involves strong air–sea coupling processes and is associated with prominent changes in rainfall, winds, SST, and sea level in the tropical Indian Ocean basin (Saji et al. 1999; Webster et al. 1999; Rao et al. 2002). Through atmospheric teleconnections, the IOD has distinct footprints on regional and global climate (Saji and Yamagata 2003). It has been shown that the IOD can affect the Indian summer monsoon (Ashok et al. 2004), Australian rainfall (Cai et al. 2011), and European weather (Saji and Yamagata

2003), and induce East African flooding and Indonesian drought (Clark et al. 2003). Through active interbasin interactions in the tropical Indo-Pacific region, ENSO and IOD can also strongly affect each other (Luo et al. 2010; Cai et al. 2019; Wieners et al. 2017, 2019; Izumo et al. 2020). Understanding the variability of the IOD, ENSO, and their relationship is thus important for climate prediction.

Existing studies have shown a significant correlation and co-occurrence between the IOD and ENSO, particularly after the mid-1970s (Baquero-Bernal et al. 2002; Xie et al. 2002; Krishnamurthy and Kirtman 2003; Annamalai et al. 2003; Meyers et al. 2007). Such connections between the IOD in the northern autumn season and other aspects of the seasonal cycle and interannual variability of Asian–Australian monsoon rainfall and eastern equatorial Pacific SSTs, have always been a central aspect of the tropospheric biennial oscillation (TBO) (Meehl 1997; Meehl and Arblaster 2002). It has been found that the negative precipitation anomalies over the western Pacific warm pool region during El Niño can induce easterly wind anomalies over the tropical Indian Ocean, contributing to development of the positive phase of the IOD (pIOD) (Annamalai et al. 2003; Shinoda et al. 2004). In addition to this variability forced by ENSO, about two-thirds of the historical IOD events have arisen as a result of Indian Ocean internal dynamics since the 1950s (Behera et al. 2006; Yang et al. 2015), in part related to mechanisms similar to those in the recharge oscillator conceptual model of ENSO (McPhaden and Nagura 2014) as well as influences from atmospheric noise forcing such as atmospheric intraseasonal oscillations (Rao and Yamagata 2004; Han et al. 2006). On the other hand, it has also been suggested that only about one-third of the IOD events occurred independently of El Niño since the 1970s (Stuecker et al. 2017). Such discrepancy is likely due to the different data analysis periods, given that IOD–ENSO correlation exhibits interdecadal variability and

[©] Supplemental information related to this paper is available at the Journals Online website: <https://doi.org/10.1175/JCLI-D-21-0085.s1>.

Corresponding author: Lei Zhang, lezh8230@colorado.edu

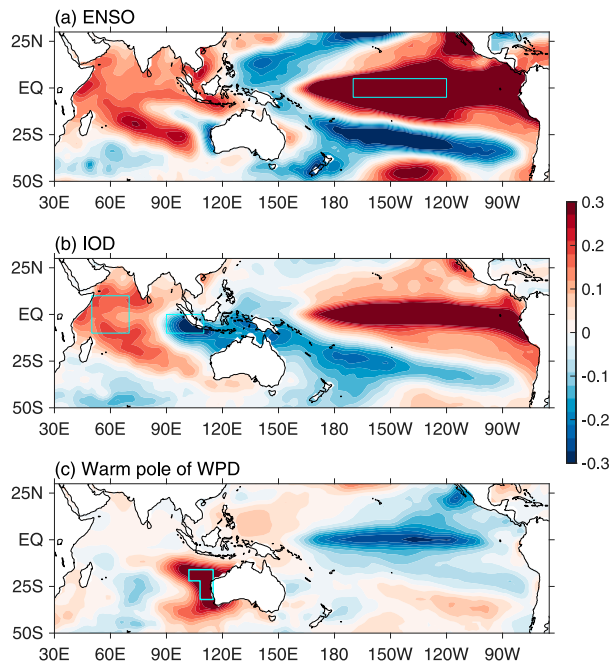


FIG. 1. Regression of SST ($^{\circ}$ C) on normalized climate mode indices using ERSSTv3b for the 1920–2010 period, showing the (a) regression of DJF-mean SST on the normalized DJF Niño-3.4 index, (b) regression of SON-mean SST on the normalized SON dipole mode index (DMI), and (c) regression of DJF-mean SST on the normalized DJF Ningaloo Niño index. Outlined boxes denote regions used to calculate the climate mode indices.

significantly increases since the mid-1970s. The less reliable data prior to the satellite era may be another reason. Conversely, it has been suggested that the pIOD could in turn contribute to the development of El Niño (Terray et al. 2016; Behera and Yamagata 2003; Luo et al. 2010; Zhang et al. 2021b) and that the pIOD played an important role in contributing to the observed extreme El Niño events of 1972/73, 1982/83, and 1997/98 (Hameed et al. 2018; Zhang et al. 2021a). The previously identified IOD–ENSO relationship has thus emphasized the simultaneous interplay between the pIOD and El Niño (or negative IOD and La Niña). By contrast, it has also been suggested that the predictability of IOD mainly originates from ENSO, while IOD does not add additional predictability to ENSO, indicating that the IOD–ENSO relationship may primarily act in one direction (Zhao et al. 2019, 2020). Hence, despite the recent progress, the impact of the IOD on the simultaneous development of ENSO, which is the focus of this study, has not been fully understood. This simultaneous impact is in addition to the previously described impact the IOD can have on ENSO development in the following year through modulating Pacific zonal wind anomalies (Izumo et al. 2010; Jourdain et al. 2016), although it has also been suggested that the IOD effect on ENSO in the following year could be part of the intrinsic ENSO cycle (Stuecker et al. 2017).

In addition to the IOD and ENSO, a regional interannual climate phenomenon was identified over the southeast Indian Ocean (SEIO) off the west coast of Australia, termed “Ningaloo Niño” (Feng et al. 2013) (Fig. 1c). It is characterized by positive

SSTA extending northwestward from the west coast of Australia into the central tropical Indian Ocean. It has been found that the southeast Indian Ocean warming can be triggered remotely by the Pacific La Niña through both the atmospheric bridge and the oceanic connection via the Indonesian passages (Feng et al. 2013; Kataoka et al. 2014; Zhang et al. 2018); in turn, the southeast Indian Ocean SST warming can strengthen the Pacific easterly trades and subsequently cause cold SSTA in the central tropical Pacific (Terray and Dominik 2005; Zhang and Han 2018). As such, this interbasin coupling yields a warm Indian Ocean–cold Pacific pattern (Zhang and Han 2018), referred to as the “warm pool dipole” (WPD), because of its proximity to the tropical Indo-Pacific warm pool (Fig. 1c) (Zhang and Han 2020). Previous studies have also shown that in addition to the close relationship with the tropical Pacific, the southeast Indian Ocean warming is sometimes associated with the pIOD forcing in the tropical Indian Ocean (Zhang and Han 2018; Zhang et al. 2018). Results from these studies imply that the IOD, WPD, and ENSO are interrelated, but the mechanisms for their interconnections remain elusive. In addition, each of these climate modes has a large impact on marine ecosystems over the Indian and Pacific Oceans (Depczynski et al. 2013; Byrne 2011). Therefore, exploring their interactions is not only important for predicting climate but also crucial for understanding and predicting marine ecosystem changes. In this study, we present a new mechanism for the pIOD to impact ENSO, in which the WPD acts as a bridge between the IOD and ENSO, and our conclusions are drawn from observational analyses combined with model experiments using a state-of-the-art climate model.

2. Data and methods

a. Observational datasets

In this study, we used the monthly SST data from the Hadley Centre Sea Ice and SST (HadISST) (Rayner et al. 2003) and Extended Reconstructed SST version 3b (ERSSTv3b) (Smith et al. 2008) to analyze the SSTA associated with ENSO and the IOD. Surface wind stress is calculated using daily surface wind data from the European Centre for Medium-Range Weather Forecasts (ECMWF) twentieth-century reanalysis (ERA-20C) (Poli et al. 2016) and formulas $\tau_x = \rho C_D |\mathbf{V}| u$ and $\tau_y = \rho C_D |\mathbf{V}| v$, where τ_x and τ_y are zonal and meridional surface wind stress, u and v denote zonal and meridional wind at 10 m, ρ is the surface air density (1.175 kg m^{-3}), and C_D is a constant drag coefficient (1.5×10^{-3}). Monthly surface shortwave radiation and surface latent heat flux data from ERA-20C are also analyzed to examine the formation mechanism of the thermocline ridge warming. For both SST and ERA-20C data, the analysis period is 1920–2010. Satellite-derived sea level data from Archiving, Validation, and Interpretation of Satellite Oceanographic (AVISO) (Ducet et al. 2000) is analyzed to compare with the CESM1 results during the satellite altimeter era from 1993 to the present. Since we focus on natural climate variations, all the anomaly fields have been detrended in this study to remove the impact of global warming. We also tried an alternative approach to remove the global warming impact by removing the regression on global mean SST at each grid point, and we

obtained similar results to those shown in this study (figure not shown).

b. CESM experiments

In this study, we analyzed the historical simulations (1920–2005) and future projections (2006–13) from the 40-member ensemble of National Center for Atmospheric Research (NCAR) Community Earth System Model, version 1 (CESM1; Hurrell et al. 2013), large ensemble (CESM1-LE) (Kay et al. 2015). In addition, we also analyzed two sets of CESM1 experiments using the same model: the Indian Ocean–Global Atmosphere (IOGA) and the Pacific Ocean–Global Atmosphere (POGA) pacemaker experiments. The simulation period is 1920–2013, using the same external forcing as the historical runs (1920–2005) from phase 5 of the Coupled Model Intercomparison Project (CMIP5) and the representative concentration pathway 8.5 (RCP8.5) experiments (2006–13). For both pacemaker experiments, a 10-member ensemble was obtained by slightly changing the initial conditions. A 10-member ensemble has been considered sufficient to isolate forced climate anomalies outside the SSTA nudging region (Kosaka and Xie 2013). Indeed, the probability density function distribution of the Niño-3.4 index is very similar between IOGA experiments and CESM1-LE (not shown), suggesting that the 10-member ensemble can capture most of the ENSO amplitude spectrum.

In the IOGA pacemaker experiments, SSTA in the tropical Indian Ocean and part of the western tropical Pacific is restored to ERSSTv3b values and added to the model SST climatology, and the rest of the global ocean is fully coupled to the atmosphere. The reason that the small domain in the western tropical Pacific is included in the nudging area is because SSTA in that region tends to covary with that in the eastern pole of the IOD. Hence, the IOGA simulations essentially synchronize the tropical Indian Ocean SSTA variability to that of the observed. The nudging region is approximately 28° – 161° E, 16° S– 14.5° N (Fig. 2), with sponge layers applied to the eastern, northern, and southern boundaries. The 10-member ensemble averaged fields of IOGA experiments are used to estimate the impacts of the pIOD on ENSO through forcing the WPD. Similarly, SSTA in the central and eastern tropical Pacific (171° – 80° W, 17° S– 15° N) is restored to observations but is fully coupled to the atmosphere elsewhere in POGA experiments, and its 10-member ensemble mean fields are utilized to explore the impacts of ENSO on the pIOD.

c. Climate modes

To document the time evolution of ENSO and IOD, climate indices are calculated using SST data from both observations and pacemaker experiments. For ENSO, the Niño-3.4 index is calculated, which is the area-averaged SSTA over the domain (170° – 120° W, 5° S– 5° N). For IOD, the dipole mode index (DMI) is defined as differences of SSTA averaged over 50° – 70° E, 10° S– 10° N and 90° – 110° E, 10° S– 0° . El Niño events are then defined as the year when the December–February (DJF)-mean Niño-3.4 index exceeds 1 standard deviation and La Niña events are defined as the year when the DJF-mean Niño-3.4 index falls below -1 standard deviation of the Niño-3.4 during 1920–2013. Similarly, positive and negative IOD events are defined as the year when the September–November (SON)-mean DMI exceeds 1 (for pIOD) or falls below -1 (for negative

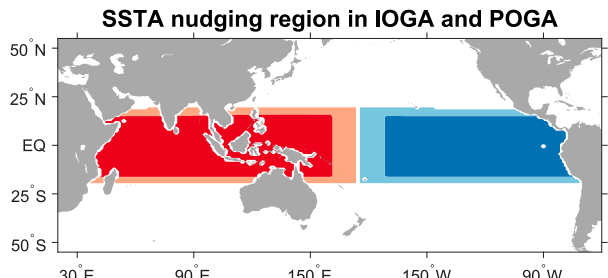


FIG. 2. Regions where SSTAs are restored to observations in the pacemaker experiments. Red is for IOGA experiments, and blue is for POGA experiments. Light colors represent the sponge layer.

IOD) standard deviation of the DMI. The selected years are shown in Fig. 3 and also in Fig. S1 in the online supplemental material. As a sensitivity test, we also tried other threshold values, such as $2/3$ standard deviation, to define both IOD and ENSO events, and obtained similar results.

We include two years that would otherwise be excluded with the selection criteria described above. For 1935, the Niño-3.4 index in the ensemble mean of IOGA pacemaker experiments is slightly below the standard deviation of the observed Niño-3.4 index but is higher than that in ensemble mean results of IOGA experiments. Therefore, this year is also selected as an El Niño year. For 1949, the Niño-3.4 index in IOGA experiments is weaker than its corresponding negative standard deviation, but that year is considered as La Niña year in the model to increase the sample size. Excluding these two years yields results that are similar to those shown in this study and therefore does not change our conclusions (figure not shown).

3. Positive IOD and El Niño

Although it has been found that El Niño and the pIOD interact and amplify each other through the atmospheric bridge in some years (Luo et al. 2010), IOD events can also occur independently from ENSO. To investigate El Niño–pIOD interactions, we analyze the two sets of pacemaker experiments and observations (Fig. 3). First, we use POGA experiments to identify whether a specific observed pIOD event is ENSO dependent or not by comparing the observed Indian Ocean SST variability with the ensemble mean of the POGA experiments. In this study a specific pIOD event is considered El Niño dependent if the amplitude of the simulated pIOD in POGA ensemble mean is at least 25% of the corresponding observed one; otherwise, it is El Niño independent. Other threshold values were also tested, and our conclusions were insensitive to the specific choice within the range of 15%–40%. After selecting the El Niño-dependent and El Niño-independent pIOD events, we then explore their diverse impacts on ENSO by analyzing the ensemble mean of IOGA experiments.

The results show that among the 20 observed pIOD events during 1920–2013, approximately one-third (seven events) are forced by the Pacific (right panel in Fig. 3a). All of these pIOD events are associated with strong eastern Pacific SST warming and six of them are classified as El Niño events (right panel in Fig. 3b), with the 1977 event showing a positive Niño-3.4 index

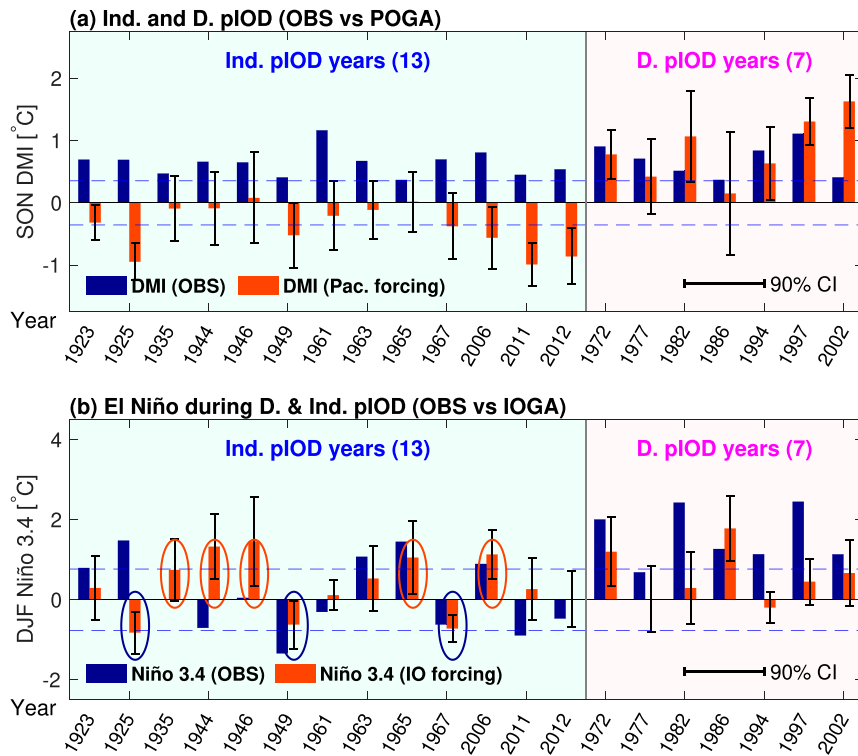


FIG. 3. (a) The SON DMI during observed pIOD years. Blue denotes DMI in observations, and red is for POGA pacemaker experiments. The pIOD years are separated into ENSO-independent events, denoted by “Ind.” (left side; 13 events) and ENSO-dependent events, denoted by “D.” (right side; 7 events), based on whether the DMI in the ensemble average of POGA experiments (which isolates the tropical Pacific forcing) exceeds 25% of the DMI in observations. The error bar denotes the uncertainty defined as 90th confidence interval across the 10 ensemble members. The blue dashed line denotes 1 standard deviation of the DMI in observations. (b) As in (a), but for DJF Niño-3.4 index during the pIOD years in observations (blue) and IOGA pacemaker experiments (red). The red ovals mark the five years when the Ind. pIOD causes El Niño, and the blue ovals mark the three years when the pIOD causes La Niña.

that is slightly below one standard deviation and the 1986 event exhibiting large uncertainty of the El Niño impact on the pIOD. A similar comparison between eastern tropical Pacific SST variability in observations and the ensemble mean of the IOGA experiments shows that more than 40% (9 of 21) of the observed El Niños are contributed by the tropical Indian Ocean forcing (Fig. S1a in the online supplemental material), and seven of them are pIOD years with the DMI exceeding one standard deviation (Fig. S1b). These results support the previous finding that El Niño and the pIOD can interact and amplify each other within the same year.

However, the ensemble mean of the IOGA experiments also shows clearly that not all pIODs favor El Niño conditions in the tropical Pacific (left panel in Fig. 3b). In particular, we note that the El Niño-dependent and El Niño-independent pIODs have apparent differences in terms of their impacts on the tropical Pacific; despite some uncertainties, the El Niño-dependent pIODs tend to favor the eastern tropical Pacific SST warming, while the impacts of the El Niño-independent pIODs on ENSO exhibit prominent event-to-event variations, with three of them actually causing strong Pacific SST cooling

(e.g., 1925, 1949, and 1967). Such diverse impacts of the pIOD on simultaneous ENSO development have not been discussed previously; however, understanding the underlying physical processes could significantly improve our understanding of the tropical Indo-Pacific interbasin coupling. Below, we focus on analyzing the causes for the diverse pIOD impacts on ENSO.

4. Diverse effects of pIOD on ENSO

Next, we first focus on the diverse impacts of the El Niño-independent pIODs on the tropical Pacific. We categorize the El Niño-independent pIODs based on whether they cause El Niño (5 pIOD–El Niño years) or La Niña (3 pIOD–La Niña years) in the ensemble mean of the IOGA experiments (years marked by ovals in Fig. 3b). Note that the selected pIOD–La Niña events are the only three pIOD years during which the ensemble mean of IOGA experiments simulates negative Niño-3.4 index, regardless of whether the pIODs are El Niño-dependent or El Niño-independent. The 1994 pIOD is an exception, showing a weak negative Niño-3.4 index in IOGA

Ind. pIOD composite in IOGA ensemble mean

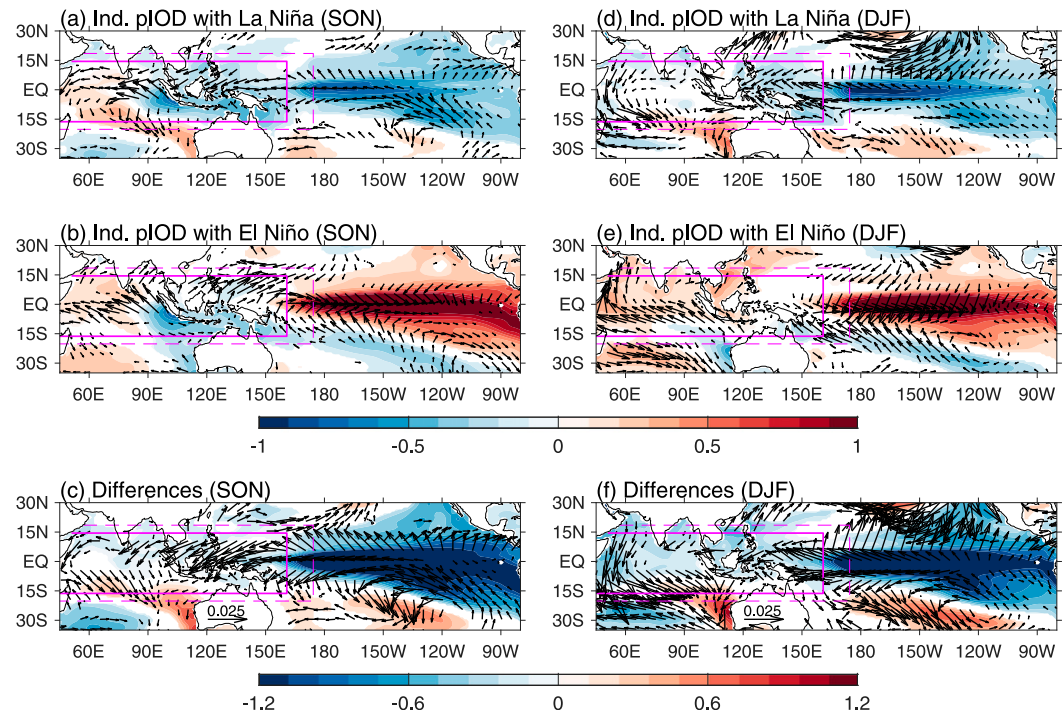


FIG. 4. Tropical Pacific anomalies induced by the El Niño-independent pIODs, as assessed by the 10-member ensemble mean results of the IOGA experiments. (a) Composite of SON mean SSTA (shading, $^{\circ}\text{C}$) and surface wind stress anomalies (vectors; N m^{-2}) during the independent pIOD events co-occurring with La Niña (1925, 1949, and 1967). (b) As in (a), but for composite of the independent pIOD events that co-occur with El Niño (1935, 1944, 1946, 1965, and 2006), and (c) the differences between (a) and (b). The purple solid-outlined box denotes the region in which SSTA is restored toward observations in the IOGA experiments, and the purple dash-outlined box denotes the sponge layer. (d)–(f) As in (a)–(c), but for the DJF season. Shown are the results that are statistically significant at the 90% confidence level.

experiments. Although there are only a few pIOD–ENSO years in our analysis, the results are obtained from a 10-member ensemble of pacemaker experiments. Since each ensemble member can be regarded as an independent realization forced with the same observed SSTA in the tropical Indian Ocean, the sample sizes are not small (30 for pIOD–La Niña and 50 for pIOD–El Niño), which boosts the statistical significance of our results. As expected, the composites of the two categories exhibit strong El Niño and La Niña signals in the tropical Pacific (Fig. 4), owing to the different pIOD forcing in the IOGA experiments. Different threshold values for selecting ENSO and IOD events, such as the 2/3 standard deviation that increases the sample size, were also tested and results are similar (not shown).

Here we focus on the SON IOD peak season when the Indian Ocean signals are the strongest, although we note that the development of associated anomalous climate conditions in the tropical Indo-Pacific basin starts in late spring/early summer, reaches maximum amplitude in SON, and quickly decays in winter (Fig. S2 in the online supplemental material). Results show that during the pIOD–El Niño years, the anomalous westward zonal SST gradient in the tropical Indian Ocean drives low-level easterly wind anomalies during SON,

along with wet anomalies over the western basin and dry anomalies over the eastern basin (Figs. 4b and 5b). The higher sea level pressure (SLP) over the eastern tropical Indian Ocean (the cold pole of the pIOD) produces an eastward pressure gradient force and thus eastward surface wind anomalies in the tropical Pacific (Fig. 4b; see also Fig. S3b in the online supplemental material), weakening the Pacific easterly trades and causing positive Pacific SSTA and rainfall anomalies (Figs. 4b and 5b). This result is in line with previous findings (Hameed et al. 2018; Behera and Yamagata 2003). On the other hand, large tropical SSTA differences between the pIOD–La Niña and pIOD–El Niño years are found in the warm pole of the pIOD over the southwest tropical Indian Ocean mean upwelling zone (7° – 15°S), where the mean thermocline is shallow (McCreary et al. 1993; Murtugudde and Busalacchi 1999) and is thus referred to as the “Seychelles–Chagos thermocline ridge” (SCTR) (Hermes and Reason 2008; Yokoi et al. 2008) (Figs. 4a,c). These results suggest that pIOD events are associated with two SSTA patterns, one with and one without warm SSTA over the thermocline ridge region. Although the warm pole of the pIOD is mainly located in the western equatorial Indian Ocean and Arabian Sea during the pIOD–El Niño years (Fig. 4b), large positive SSTAs and rainfall anomalies also

Ind. pIOD composite in IOGA ensemble mean

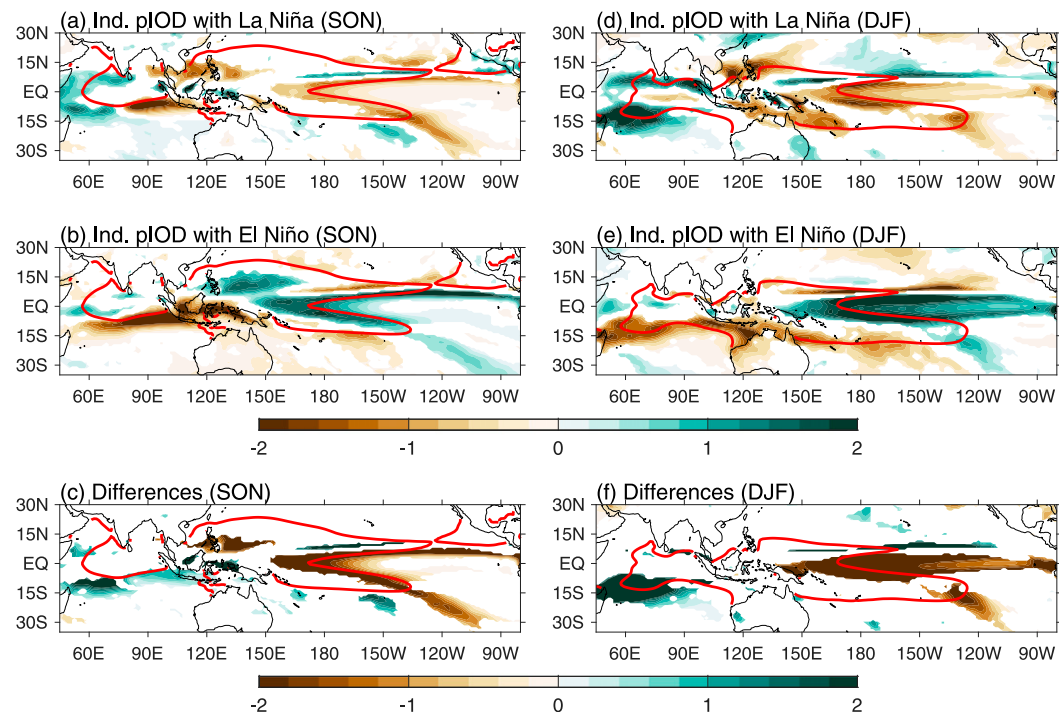


FIG. 5. As in Fig. 4, but for precipitation anomalies (shading; mm day^{-1}). Red lines represent the 27°C contour for seasonal-mean SST climatology.

appear in the southwestern tropical Indian Ocean in the vicinity of the thermocline ridge during the pIOD-La Niña (Figs. 4a,c and 5a,c). These warm anomalies induce an anomalous interhemispheric SST gradient that drives surface northerly wind anomalies over the tropical Indian Ocean to strengthen the northeast monsoon circulation.

Note that the warming in the thermocline ridge region during the pIOD-La Niña extends to the southeast Indian Ocean (warm pole of the positive WPD) (Figs. 1c and 4a,c). This is because the pIOD SSTAs with thermocline ridge warming induce both easterly wind anomalies near the equator and northerly wind anomalies in basin interior south of the equator, leading to strong anticyclonic wind anomalies over the tropical south Indian Ocean with the northerly wind anomalies extending to the subtropics in the southeast basin off the west coast of Australia (Zhang et al. 2018). These northerly winds weaken the mean-state southerly winds in the region and cause prominent southeast Indian Ocean warming (Kataoka et al. 2014; Marshall et al. 2015; Zhang et al. 2018). The role of the pIOD in causing southeast Indian Ocean warming has been confirmed through both observational analysis and model experiments (Zhang et al. 2018) and is consistent with the IOGA results shown here. We also carried out two sensitivity experiments using an atmospheric general circulation model forced with the two tropical Indian Ocean pIOD STA patterns, one with and one without thermocline ridge warming. Results indeed show that the pIOD with thermocline ridge warming

produces northerly wind anomalies in the southeast Indian Ocean that weaken the background southerly winds and opposite for the pIOD without the thermocline ridge warming (Fig. S4 in the online supplemental material), further confirming our above argument based on the IOGA experiments. Although the coastal wind anomalies are relatively weak in the atmospheric model, they can kick start positive feedback associated with the air-sea coupling, which then strengthen both wind and SST anomalies in the southeast Indian Ocean.

Consistent with the patch of positive STA in the south Indian Ocean, positive sea level anomalies are also found in the Ningaloo Niño region (Fig. S5 in the online supplemental material), which indicate an anomalously deep thermocline that may contribute to the SST warming. Changes in horizontal ocean currents on the other hand are weak and therefore do not seem to play an important role (not shown). To further validate our results, we compare the CESM1 results with the high-quality satellite-derived global sea level data. Note that there is no pIOD-La Niña case found during the satellite altimeter era of 1993 to the present (Fig. 3b). Instead, we compared the pIOD events that caused weak warming (or cooling) and strong warming in tropical Pacific in the ensemble mean of IOGA and found increased southeast Indian Ocean sea level in the former relative to the latter composite in both IOGA and satellite altimeter data (Fig. S6 in the online supplemental material), further supporting our above conclusions. We note that the corresponding POGA experiments also show increased sea

Ind. pIOD composite in observations

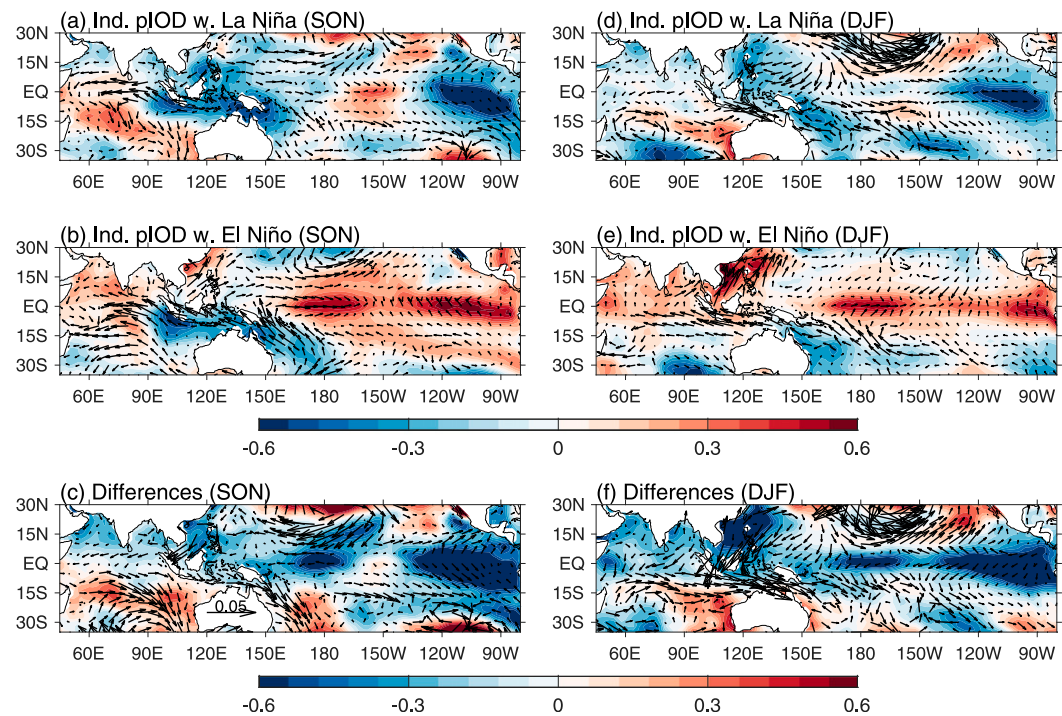


FIG. 6. Composites of SST (shading: $^{\circ}\text{C}$) and surface wind stress (vector; N m^{-2}) anomalies using ERSSTv3b and ERA-20C datasets, respectively. Selected years are the same as in Fig. 4.

level along north and west Australian coasts, suggesting some contribution from ENSO.

Both observations and model experiments have shown that the southeast Indian Ocean warming induces negative SLP anomalies that extend to the western tropical Pacific, which subsequently enhance the zonal SLP gradient in the tropical Pacific and thereby strengthen the mean state easterly winds (Terray and Dominiak 2005; Zhang and Han 2018). The stronger trade winds then cause cold Pacific SSTA through enhancing the surface evaporation (Morioka et al. 2012) and upwelling, leading to the formation of the positive WPD, namely a warm Indian Ocean and cold Pacific Ocean. This is consistent with the La Niña-like conditions in the tropical Pacific in the IOGA experiments (Fig. 4a). These results suggest that the WPD acts as a bridge that transmits the pIOD impact to the tropical Pacific. Note that POGA experiments show that the observed Pacific cold SSTAs during the pIOD-La Niña years do not induce significant warm SSTAs in the southeast Indian Ocean (Fig. S7 in the online supplemental material), also supporting the idea that the positive SSTAs off the western Australian coast in Fig. 4a is caused by pIOD SSTAs with an SCTR warming pattern. It is also worth emphasizing that the thermocline ridge warming itself is not a direct cause for the La Niña, since it tends to induce weak warming in the tropical Pacific based on the IOGA experiments (Fig. S8 in the online supplemental material). Further, atmospheric model experiments also show that warm/cold

SSTA in the thermocline ridge region alone does not significantly affect the tropical Pacific winds (Fig. S9 in the online supplemental material).

During DJF, the pIOD decays while the SSTA in the tropical Pacific and the southeast Indian Ocean continues to develop (Figs. 4d–f), owing to local air-sea coupling as well as interbasin interactions (Terray and Dominiak 2005; Zhang and Han 2018). Meanwhile, El Niño is associated with basin-scale warming in the tropical Indian Ocean during DJF and La Niña with Indian Ocean cooling (Klein et al. 1999), and earlier studies also showed that the Indian Ocean basinwide warming—if it is caused by processes other than enhanced subsidence—can cool the tropical Pacific and Indian Ocean cooling favors Pacific warming (Ohba and Ueda 2007; Morioka et al. 2012; Zhang et al. 2019). Hence, although the ensemble mean of IOGA pacemaker experiments is supposed to isolate the impact of tropical Indian Ocean SST variability, the basin-scale SSTA does not seem to play a role in forcing the Pacific wind and SST anomalies *after the IOD peak*. Instead, SSTA in the tropical Pacific is closely connected with SSTA in the southeast Indian Ocean during DJF, which mainly results from the pIOD forcing *from the previous season*.

The above IOGA results agree with observations (Fig. 6). In observed pIOD years, La Niña-like conditions appear in the tropical Pacific when there is southeast Indian Ocean warming off the west coast of Australia accompanied by the thermocline ridge warming (Figs. 6a and 6c). By contrast, without those warming signals, prominent positive SSTA is evident in the

tropical Pacific (Fig. 6b). Observed precipitation anomalies overall agree with IOGA results as well (Fig. S10 in the online supplemental material). There are also some noticeable differences between observations and IOGA experiments, such as the strong northerly wind anomalies in the western tropical Indian Ocean in the model results (Fig. 4a) that are weak or absent in the observations (Fig. 6a), which could be due to influences of other factors such as anomalous Indian monsoon system. Nevertheless, since the ensemble average of the IOGA experiments filters out the impacts of internal climate variability outside the tropical Indian Ocean, the agreement between the ensemble mean of IOGA and observations (cf. Figs. 4 and 6) suggests that the observed changes in the tropical Pacific during the selected pIOD years are indeed due to the Indian Ocean forcing. There are a few exceptions, such as in 1925, during which the IOGA simulates a La Niña event, while it was an El Niño year in observations (Fig. 3b). This is because ENSO is a strong internal mode of climate variability, and El Niño event still occurred in 1925 albeit with strong forcing from pIOD. Because 1925 was included in the composites of Figs. 4a and 6a, weak warming was shown in the central tropical Pacific in Fig. 6a but was absent from Fig. 4a. Similarly, 1944 was a La Niña year, opposite to the IOGA result. These inconsistencies suggest that in some years processes other than the tropical Indo-Pacific interactions can play a dominant role, such as forcings from the extratropical Pacific that may trigger ENSO (Chang et al. 2007; Alexander 2010; Zhang et al. 2014). This is also one of the reasons why the ENSO–IOD correlation is overall not high and nonstationary.

The above analysis focuses on the El Niño–independent pIODs. We also extended our analysis to the El Niño–dependent pIODs, which overall tend to cause positive SSTA in the tropical Pacific but with noticeably different warming magnitudes (Fig. 3b). Consistent with the conclusions above, we find that for the pIODs with warming in the thermocline ridge and the southeast Indian Ocean, the Pacific warming is prominently weakened (Fig. S11 in the online supplemental material). Taking all the pIODs into consideration (both El Niño–dependent and El Niño–independent events), the key role of the thermocline ridge warming and the WPD in affecting the diverse impacts of the pIOD on ENSO is still evident (Fig. S12 in the online supplemental material).

As a comparison, we also analyzed results from the 40-member ensemble of the CESM1-LE during the same period as our pacemaker experiments (1920–2013). After removing the ensemble mean results that isolate the climate anomalies forced by external forcing (both anthropogenic and natural), we selected the pIOD events that co-occur with La Niña (72) and El Niño (501), respectively (Fig. S13 in the online supplemental material). We found that the pIOD–La Niña events also correspond to prominent warming in the thermocline ridge that extends to the southeast Indian Ocean, while the pIOD–El Niño events do not. Hence, CESM1-LE results also support our conclusions above. In addition, the CESM1-LE also seems to simulate weaker cold pole in the eastern tropical Indian Ocean during pIOD–La Niña years relative to pIOD–El Niño years, which may also contribute to the opposite Pacific anomalies between the two composites. However, since the differences in the SSTAs at the cold pole are negligible in

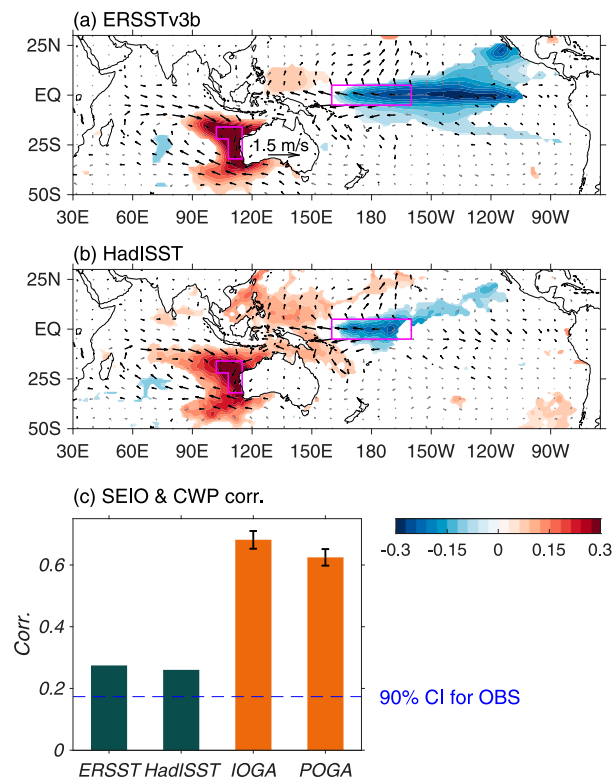


FIG. 7. (a) Regression of DJF SST (shading; $^{\circ}$ C) and surface wind anomalies (vector; $m s^{-1}$) on normalized DJF SEIO SST index using ERSSTv3b. Shown are results that are 90% statistically significant. Black vectors denote the wind regressions that are significant at the 90% confidence level. The two outlined regions are used to calculate the SEIO index (102° – 108° E, 22° – 16° S and 108° – 115° E, 32° – 16° S) and the central-western Pacific index (CWPI; 160° E– 160° W, 5° S– 5° N). (b) As in (a), but for HadISST results. (c) Correlation coefficient between the DJF SEIO index and DJF CWPI in ERSSTv3b, HadISST, and the average of each ensemble members from IOGA and POGA experiments. The signs are flipped. The blue dashed line represents the 90% confidence level for the two observational datasets. Vertical lines represent 90% confidence interval for results from IOGA and POGA experiments.

observations (Fig. 4c), the contrasting pIOD impacts on ENSO that we found in observations and the IOGA experiments are not due to different amplitudes of the cold SSTAs in the eastern tropical Indian Ocean.

5. Interbasin interaction and the WPD

The interaction between the southeast Indian Ocean warming and the tropical Pacific cooling is crucial for pIODs with thermocline ridge warming to cause Pacific La Niña–like conditions. The associated interbasin coupling processes (Zhang and Han 2018) indicate that the positive SSTA in the tropical–subtropical southeast Indian Ocean induces negative SLP anomalies that extend to the Maritime Continent as atmospheric Kelvin wave, increasing the zonal SLP gradient in the tropical Pacific and thereby strengthening the Pacific easterly trades (Fig. 7).

Consequently, SST in the central tropical Pacific decreases due to enhanced surface evaporation (Morioka et al. 2012), upwelling, and zonal advection. The negative SSTA in the tropical Pacific further enhances the easterly trade winds to its west through local air-sea coupling, which subsequently enhance the Indonesian Throughflow (ITF) and thus contribute to the SST warming in the southeast Indian Ocean (Kataoka et al. 2014; Tozuka et al. 2014). Through the atmospheric bridge, the Pacific cold SSTA can also enhance the anomalous cyclonic winds over the eastern subtropical Indian Ocean, which is south of the anticyclone of the tropical south Indian Ocean (Figs. 4 and 6), and thereby further enhances the coastal SST warming (Zhang et al. 2018).

Here we briefly revisit the close connection between the southeast Indian Ocean and the tropical Pacific by conducting an observational linear regression analysis (Figs. 7a,b). The results show that SST warming in the southeast Indian Ocean is indeed associated with strong cooling anomalies in the western-central tropical Pacific; meanwhile, cyclonic wind anomalies appear in the south Indian Ocean, and easterly trades are enhanced over the western tropical Pacific. Consistently, the observed SSTA averaged over the two regions shows a negative correlation (Fig. 7c). Although the correlation is not very high (-0.27) because of its strong decadal variation (not shown), it is statistically significant at the 90% confidence level. Strong negative correlations are found in IOGA and POGA pacemaker experiments, further supporting the strong interbasin coupling. Note that the model tends to overestimate the correlations, which could be due to the too-strong western-central tropical Pacific SSTA variability in the model (Fig. 10) that may result in too-strong negative Pacific SSTAs associated with the southeast Indian Ocean warming. A composite analysis of the pacemaker experiments also suggests that the southeast Indian Ocean warming and the Pacific cooling anomalies tend to co-occur (not shown), as found in observations. We note that the two observational SST datasets also show some differences. For instance, the Pacific cold SSTA associated with the WPD extends to the eastern tropical Pacific in ERSST but not in HadISST, and such discrepancy could be due to sparse observations prior to the 1950s in the region (Deser et al. 2010).

6. Thermocline ridge warming

The Indian Ocean thermocline ridge is the other key region that connects the tropical and the southeast Indian Ocean. Note that although the warm SSTA in the thermocline ridge region does not seem strong ($<0.4^{\circ}\text{C}$), it causes prominent atmospheric responses, including enhanced precipitation in the SCTR region because the SCTR resides in atmospheric intertropical convergence zone where mean SST is high ($>27^{\circ}\text{C}$) during boreal autumn–winter (Li et al. 2014) (Fig. 5). Here we analyze the physical causes for the thermocline ridge warming during selected pIOD-La Niña years. As previously discussed, the thermocline ridge warming induces an anomalous interhemispheric SST gradient, which drives northerly and northwesterly wind anomalies over the south Indian Ocean (Fig. 4). Our observational analysis shows that the positive SSTA is primarily caused by the reduced surface wind speed

and subsequently the weakened surface latent heat flux loss (Figs. 8a,d), consistent with previous findings (Foltz et al. 2010). These anomalies are in turn associated with northwesterly wind anomalies counteracting the mean southeasterly winds over the south Indian Ocean between 10° and 15°S . Hence, the development of the thermocline ridge warming and the associated northerly wind anomalies are mainly due to a positive feedback: the wind-evaporation-SST (WES) mechanism (Xie and Philander 1994). The enhanced downward Ekman pumping velocity in the western part of the thermocline ridge (Fig. 8j) may also help enhance the warm SSTA at the SCTR by reducing the mean upwelling cooling, while the surface solar radiation anomalies tend to cool down the thermocline ridge region (Fig. 8c), which could be due to the increased cloudiness caused by the surface warming.

Since the SCTR warming is part of the pIOD warm pole, it is key to separating the pIOD into two types that have opposite effects on ENSO. While the development of the warm SSTAs in the SCTR region is primarily due to the WES mechanism, the initial warming of the warm pole at the SCTR region (or lack thereof) may be related to other Indian Ocean internal processes, such as the anomalous atmospheric monsoon circulation, or oceanic wave processes. Previous studies have suggested that the thermocline ridge warming could be caused by El Niño forcing from the preceding season (Klein et al. 1999; Xie et al. 2002; Huang and Kinter 2002; Rao and Behera 2005). For the pIOD-La Niña events, however, analysis of the ensemble mean of POGA experiments shows that the observed Pacific SSTA tends to cause negative IOD along with thermocline ridge cooling (Figs. S7a–d in the online supplemental material). This result suggests that the thermocline ridge warming associated with the pIOD-La Niña events is induced by Indian Ocean internal processes.

7. Summary and discussion

Through analysis of observational datasets and numerical experiments using a state-of-the-art climate model, we investigate the impacts of the pIOD on the simultaneous development of ENSO. Our results show that approximately one-third of the historical pIOD events are forced by El Niño, and they in turn tend to amplify El Niño. This result seems consistent with some of the previous findings (Behera et al. 2006; Yang et al. 2017), but different from the studies that use observational data in more recent periods (e.g., Stuecker et al. 2017). The discrepancy could be attributable to the decadal variations in the IOD-ENSO relationship and/or data quality issue during the early twentieth century due to the sparse observations. Furthermore, although changes in the IOD-ENSO correlation may be due to decadal variations in the ENSO variance and changes in the ENSO flavors (Zhang et al. 2015), its causes may need further investigation. In addition, the IOGA experiments also show that 45% of the pIOD events were followed by La Niña in the next year in the model (not shown), which is consistent with the previous finding that a pIOD may favor La Niña in the following year (Izumo et al. 2010).

Different from the El Niño-dependent pIODs, the effect of the El Niño-independent pIODs on the tropical Pacific varies

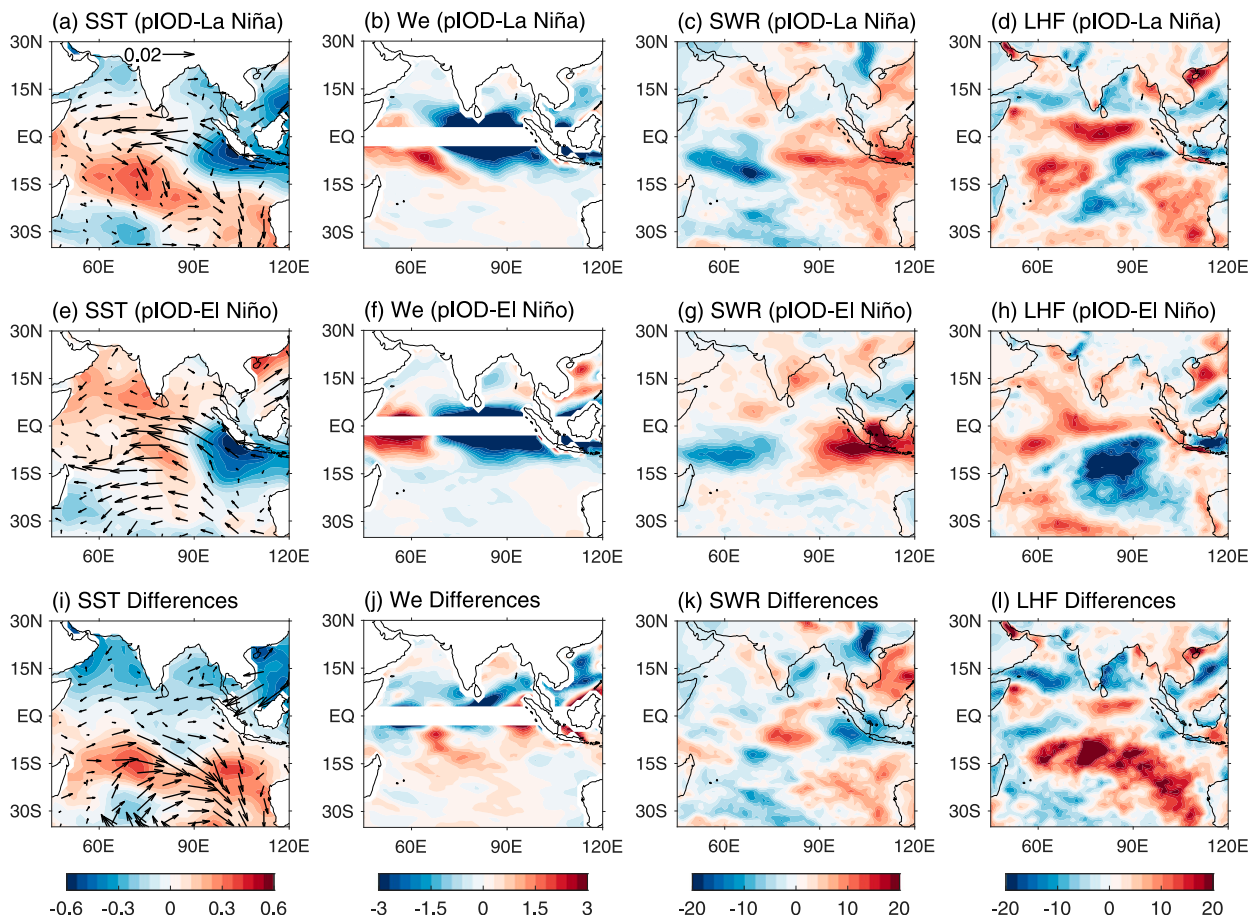


FIG. 8. Composites of observational SON mean (a) SST ($^{\circ}$ C) and surface wind stress anomalies ($N m^{-2}$), (b) Ekman pumping velocity (W_e ; $10^{-6} m s^{-1}$), (c) surface shortwave radiation anomalies (SWR; $W m^{-2}$), and (d) surface latent heat flux anomalies (LHF; $W m^{-2}$) during independent pIODs that cause La Niña. (e)–(h) As in (a)–(d), but for composites of independent pIODs that cause El Niño. (i)–(l) Differences between the two composites.

considerably. Of 13 independent pIODs, five favor El Niño and three favor La Niña, which is in contrast to the simultaneous interplay between El Niño and the pIOD documented by previous studies (Baquero-Bernal et al. 2002; Krishnamurthy and Kirtman 2003; Annamalai et al. 2003; Meyers et al. 2007). Interestingly, the pIOD-La Niña years identified in this study occur prior to the 1970s whereas the pIOD-El Niño years occur in recent decades, consistent with the higher DMI-Niño-3.4 correlation since the 1980s (Stuecker et al. 2017); prior to that, however, the observed IOD-ENSO correlation is generally lower, although the uncertainty is also larger due to the low data quality. Meanwhile, it is worth noting that the uncertainties in the SSTA forcing themselves do not affect the associated physical mechanisms simulated in the model, because the IOGA experiments mainly simulate the different responses of the tropical Pacific Ocean to the different pIOD SSTA patterns shown in the observations.

The diverse effects of pIODs on ENSO are primarily associated with two types of pIOD SSTA patterns, one with and the other without thermocline ridge warming in the western pole. The pIODs with thermocline ridge warming induce anomalous

interhemispheric SST gradients that drive northerly wind anomalies over the south Indian Ocean (upper panel of Fig. 9a). The northerly wind anomalies weaken the prevailing southeasterlies, further causing SST warming in the thermocline ridge and over the southeast Indian Ocean off the west coast of Australia, where local air-sea interaction gives rise to cyclonic wind anomalies to the west in subtropics, which is south of the anticyclonic wind associated with the pIOD in the tropics (lower panel of Fig. 9a).

Through the Indo-Pacific interbasin coupling mechanism associated with the “warm pool dipole” (WPD), the southeast Indian Ocean warming causes La Niña-like conditions in the tropical Pacific (Fig. 9a, lower panel). The cold central tropical Pacific can in turn enhance warm southeast Indian Ocean through both the atmospheric bridge and the oceanic connection, and the out-of-phase SSTAs in the two regions together form a positive feedback loop (Zhang and Han 2018, 2020). By contrast, the pIOD with strongest SST warming occurring in the western equatorial basin and the Arabian Sea tends to warm the tropical Pacific and thus favors El Niño-like conditions through the large-scale east-west circulation in the

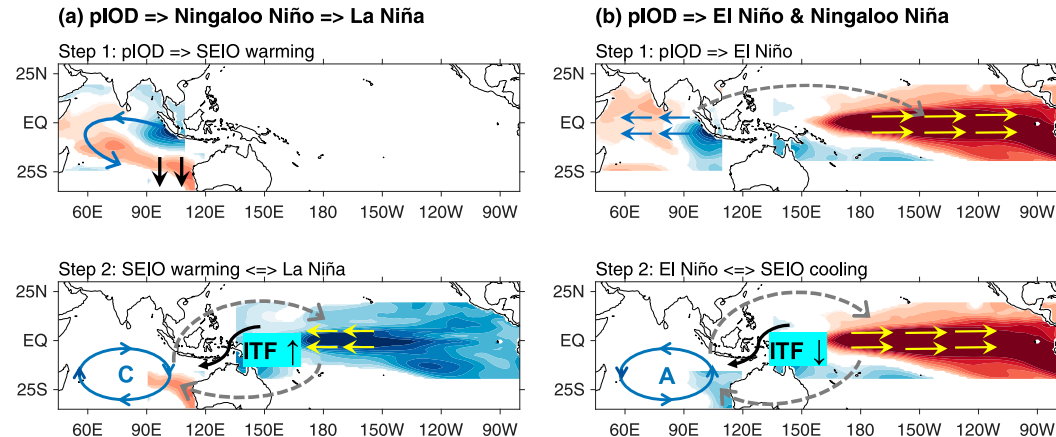


FIG. 9. Schematic diagram that illustrates different impacts of the pIOD on SEIO and the tropical Pacific. Arrows denote low-level wind anomalies, and shading represents SSTAs. (a) pIOD with thermocline ridge warming induces anticyclonic wind anomalies over the south Indian Ocean, which favors the SEIO warming (top plot). The SEIO warming induces the tropical Pacific cooling through enhanced trade winds (bottom plot). The Pacific cooling anomalies in turn favors the southeast Indian ocean warming through atmospheric bridge (cyclonic wind anomalies over the south Indian Ocean) and the oceanic connection (enhanced ITF). (b) pIOD without thermocline ridge warming induces El Niño-like conditions through causing westerly anomalies over the tropical Pacific. El Niño may subsequently cause negative SSTAs in the SEIO through the oceanic connection and the atmospheric bridge, which in turn favors El Niño.

atmosphere as that involved with the TBO (Meehl 1997; Meehl and Arblaster 2002) (Fig. 9b). Note that although the cold pole of the pIOD suppresses the local precipitation in both types of the pIOD (Fig. 5), which tends to cause westerly wind anomalies over the tropical Pacific, this effect is much weakened by the thermocline ridge warming. This is also likely the reason why the southeast Indian Ocean warming during the pIOD–La Niña years is more efficient in strengthening the Pacific easterly winds (Fig. 9a).

While the WPD can act as a bridge that transmits diverse pIOD impacts on ENSO, whether the pIOD can cause the southeast Indian Ocean warming (warm pole of the WPD) depends on the presence of warm SSTAs over the thermocline ridge in the western pole of the pIOD, the formation of which is strongly influenced by latent heat flux and amplified by the wind–evaporation–SST feedback. In addition, reduced upwelling due to deepened thermocline may also play some role. Note that composites of thermocline ridge warming/cooling alone (without pIOD) in IOGA experiments show negligible SSTAs in the southeast Indian Ocean (Fig. S8 in the online supplemental material). It is the pIOD with thermocline ridge warming that produces easterly wind anomalies along the equator and northerly wind anomalies in the basin interior, leading to the strong anticyclonic wind anomalies over the tropical south Indian Ocean with northerly winds extending to the southeast Indian Ocean off the west coast of Australia. These wind anomalies cause warm SSTAs that subsequently affect the tropical Pacific. It is noteworthy that both Ningaloo Niño and the WPD can also occur without the pIOD and affect ENSO independently (Zhang et al. 2018).

While this study focuses on pIOD events, we have also analyzed the effects of negative IODs (nIODs). The results show

that while nIODs may also have different effects on ENSO, the cause is different from the reasons discussed above for pIODs. It seems that the nIODs with stronger warming in the eastern pole tend to favor La Niña, whereas those with strong cooling in the western pole correspond to El Niño in IOGA (not shown). Because of the asymmetry between the pIODs and nIODs in terms of their effects on ENSO, here we only focus on the pIOD and will explore the effects of nIODs on ENSO in a future study.

As discussed above, in this study we examine the ENSO–IOD relationship by combining observational analysis and climate model experiments. However, it is worth noting that there are well-known biases in simulated tropical climate modes from the current generation of climate models. For instance, it has been found that the SST variability in the eastern Indian Ocean is overly large in the model in comparison with observations (Weller and Cai 2013). Since the tropical Indian Ocean SST in IOGA pacemaker experiments is restored toward observations, such model biases are reduced to some degree in the results presented above. Outside the SST nudging region, the pacemaker experiments fully represent atmosphere–ocean coupling processes, which is important because positive air–sea feedback plays a crucial role in the development of tropical climate variabilities (Bjerknes 1969). But model biases, such as the well-known cold tongue bias, may affect the simulated processes in those regions. Indeed, the IOGA and POGA experiments seem to overestimate the SST variability outside the nudging region including the western tropical Pacific region, and the ENSO–IOD correlation is also exaggerated in comparison with observations (Fig. 10), similar to the biases found in other climate models (Jourdain et al. 2016). Such model biases indicate that the pIOD impact on ENSO found in this study

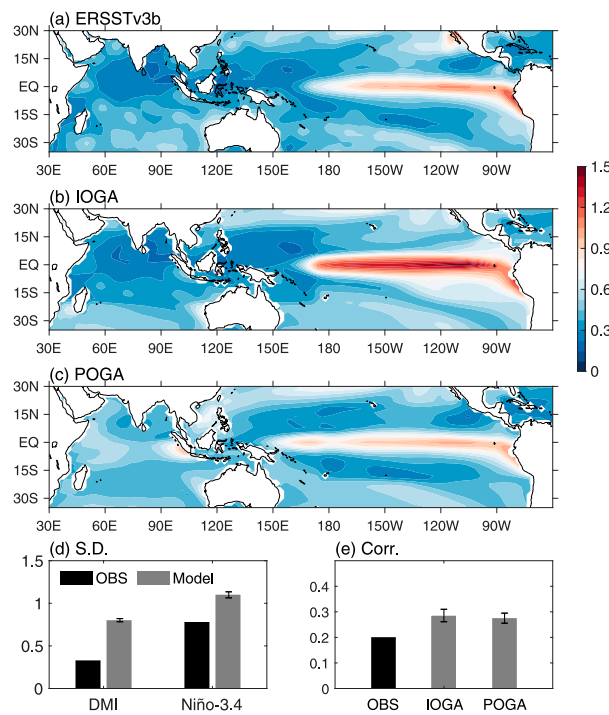


FIG. 10. (a) Standard deviation of SSTA in (a) observations ($^{\circ}$ C) using ERSSTv3 and the (b) IOGA and (c) POGA experiments. The standard deviations were calculated for each ensemble member, and shown are the averaged results. (d) Standard deviation of DMI and Niño-3.4 in observations and the model counterpart (DMI in POGA and Niño-3.4 in IOGA). (e) The DMI–Niño-3.4 correlation in observations and pacemaker experiments. The vertical bars in (d) and (e) represent uncertainty across ensemble members, which is defined as the 90% confidence interval.

could be overestimated. On the other hand, the selected pIOD–La Niña and pIOD–El Niño years show overall good agreement between the pacemaker experiments and observations (Figs. 4 and 5), which lends more confidence to our conclusions that the pIOD contributes to the development of ENSO in those years. Note also that there are uncertainties in the observational datasets used in this study as well, especially prior to the satellite era (Deser et al. 2010), which could lead to biases in the observed ENSO–IOD relationship. Hence, the model–data agreement also needs to be treated with caution.

Different from previous understanding, our results show that the pIOD not only can contribute to the development of El Niño, but also could in some circumstances favor La Niña–like conditions, with the latter scenario being associated with warm SSTA over the thermocline ridge and the southeast Indian Ocean. It is thus important to consider detailed SSTA patterns in the tropical Indian Ocean to understand and predict its impacts on the tropical Pacific. While the SON SSTA associated with a pIOD without strong thermocline ridge warming may serve as a predictor for enhanced DJF El Niño, a pIOD pattern with strong thermocline ridge warming extending to the southeast basin may serve as a predictor for La Niña. Future climate prediction should take into consideration the

diverse SSTA patterns of the IOD, and their different interactions with the WPD and ENSO.

Acknowledgments. Authors Han and Zhang are supported by NSF AGS 1935279, NASA Ocean Surface Topography Science Team NNX17AI63G and 80NSSC21K1190, and NSF OCE 1658132. Portions of this study were supported by the Regional and Global Model Analysis (RGMA) component of the Earth and Environmental System Modeling Program of the U.S. Department of Energy’s Office of Biological and Environmental Research (BER) via National Science Foundation IA 1844590. Computing resources (<https://doi.org/10.5065/D6RX99HX>) were provided by the Climate Simulation Laboratory at NCAR’s Computational and Information Systems Laboratory, sponsored by the National Science Foundation and other agencies. Author Shinoda is supported by NSF Grant OCE-1658218, NASA Grant NNX17AH25G, NOAA Grant NA17OAR4310256, and DoD Grant W911NF-20-1-0309. The National Center for Atmospheric Research is sponsored by the National Science Foundation. This is PMEL Contribution No. 5075. All data needed to evaluate the conclusions in the paper are present in the paper and/or the online supplemental material. Additional data are available from the authors upon request.

REFERENCES

Alexander, M., 2010: Extratropical air–sea interaction, sea surface temperature variability, and the Pacific decadal oscillation. *Climate Dynamics: Why Does Climate Vary?*, Geophys. Monogr., Vol. 189, Amer. Geophys. Union, 123–148, <https://doi.org/10.1029/2008GM000794>.

—, I. Bladé, M. Newman, J. R. Lanzante, N.-C. Lau, and J. D. Scott, 2002: The atmospheric bridge: The influence of ENSO teleconnections on air–sea interaction over the global oceans. *J. Climate*, **15**, 2205–2231, [https://doi.org/10.1175/1520-0442\(2002\)015<2205:TABTIO>2.0.CO;2](https://doi.org/10.1175/1520-0442(2002)015<2205:TABTIO>2.0.CO;2).

Annamalai, H., R. Murtugudde, J. Potemra, S.-P. Xie, P. Liu, and B. Wang, 2003: Coupled dynamics over the Indian Ocean: Spring initiation of the zonal mode. *Deep-Sea Res. II*, **50**, 2305–2330, [https://doi.org/10.1016/S0967-0645\(03\)00058-4](https://doi.org/10.1016/S0967-0645(03)00058-4).

Ashok, K., Z. Guan, N. H. Saji, and T. Yamagata, 2004: Individual and combined influences of ENSO and the Indian Ocean dipole on the Indian summer monsoon. *J. Climate*, **17**, 3141–3155, [https://doi.org/10.1175/1520-0442\(2004\)017<3141:IACIOE>2.0.CO;2](https://doi.org/10.1175/1520-0442(2004)017<3141:IACIOE>2.0.CO;2).

Baquero-Bernal, A., M. Latif, and S. Legutke, 2002: On dipole like variability of sea surface temperature in the tropical Indian Ocean. *J. Climate*, **15**, 1358–1368, [https://doi.org/10.1175/1520-0442\(2002\)015<1358:ODVOSS>2.0.CO;2](https://doi.org/10.1175/1520-0442(2002)015<1358:ODVOSS>2.0.CO;2).

Behera, S. K., and T. Yamagata, 2003: Influence of the Indian Ocean dipole on the Southern Oscillation. *J. Meteor. Soc. Japan*, **81**, 169–177, <https://doi.org/10.2151/jmsj.81.169>.

—, J. J. Luo, S. Masson, S. A. Rao, H. Sakuma, and T. Yamagata, 2006: A CGCM study on the interaction between IOD and ENSO. *J. Climate*, **19**, 1688–1705, <https://doi.org/10.1175/JCLI3797.1>.

Bjerknes, J., 1969: Atmospheric teleconnections from the equatorial Pacific. *Mon. Wea. Rev.*, **97**, 163–172, [https://doi.org/10.1175/1520-0493\(1969\)097<0163:ATFTEP>2.3.CO;2](https://doi.org/10.1175/1520-0493(1969)097<0163:ATFTEP>2.3.CO;2).

Byrne, M., 2011: Impact of ocean warming and ocean acidification on marine invertebrate life history stages: Vulnerabilities and potential for persistence in a changing ocean. *Oceanography and Marine Biology: An Annual Review*, R. N. Gibson, R. J. A.

Atkinson, J. D. M. Gordon, Eds., CRC Press, 1–42, <https://doi.org/10.1201/b11009>.

Cai, W., P. van Renssch, T. Cowan, and H. H. Hendon, 2011: Teleconnection pathways of ENSO and the IOD and the mechanisms for impacts on Australian rainfall. *J. Climate*, **24**, 3910–3923, <https://doi.org/10.1175/2011JCLI4129.1>.

—, and Coauthors, 2019: Pan-tropical climate interactions. *Science*, **363**, eaav4236, <https://doi.org/10.1126/science.aav4236>.

Chang, P., L. Zhang, R. Saravanan, D. J. Vimont, J. C. H. Chiang, L. Ji, H. Seidel, and M. K. Tippett, 2007: Pacific meridional mode and El Niño–Southern Oscillation. *Geophys. Res. Lett.*, **34**, L16608, <https://doi.org/10.1029/2007GL030302>.

Clark, C. O., P. J. Webster, and J. E. Cole, 2003: Interdecadal variability of the relationship between the Indian Ocean zonal mode and East African coastal rainfall anomalies. *J. Climate*, **16**, 548–554, [https://doi.org/10.1175/1520-0442\(2003\)016<0548:IVOTRB>2.0.CO;2](https://doi.org/10.1175/1520-0442(2003)016<0548:IVOTRB>2.0.CO;2).

Depczynski, M., and Coauthors, 2013: Bleaching, coral mortality and subsequent survivorship on a West Australian fringing reef. *Coral Reefs*, **32**, 233–238, <https://doi.org/10.1007/s00338-012-0974-0>.

Deser, C., A. S. Phillips, and M. A. Alexander, 2010: Twentieth century tropical sea surface temperature trends revisited. *Geophys. Res. Lett.*, **37**, L10701, <https://doi.org/10.1029/2010GL043321>.

Ducet, N., P. Y. Le Traon, and G. Reverdin, 2000: Global high-resolution mapping of ocean circulation from TOPEX/Poseidon and ERS-1 and -2. *J. Geophys. Res. Oceans*, **105**, 19477–19498, <https://doi.org/10.1029/2000JC900063>.

Feng, M., M. J. McPhaden, S. P. Xie, and J. Hafner, 2013: La Niña forces unprecedented Leeuwin Current warming in 2011. *Sci. Rep.*, **3**, 1277, <https://doi.org/10.1038/srep01277>.

Foltz, G. R., J. Vialard, B. Praveen Kumar, and M. J. McPhaden, 2010: Seasonal mixed layer heat balance of the southwestern tropical Indian Ocean. *J. Climate*, **23**, 947–965, <https://doi.org/10.1175/2009JCLI3268.1>.

Hameed, S. N., D. Jin, and V. Thilakan, 2018: A model for super El Niños. *Nat. Commun.*, **9**, 2528, <https://doi.org/10.1038/s41467-018-04803-7>.

Han, W., G. A. Meehl, and A. Hu, 2006: Interpretation of tropical thermocline cooling in the Indian and Pacific Oceans during recent decades. *Geophys. Res. Lett.*, **33**, L23615, <https://doi.org/10.1029/2006GL027982>.

Hermes, J. C., and C. J. C. Reason, 2008: Annual cycle of the South Indian Ocean (Seychelles–Chagos) thermocline ridge in a regional ocean model. *J. Geophys. Res. Oceans*, **113**, C04035, <https://doi.org/10.1029/2007JC004363>.

Huang, B., and J. L. Kinter III, 2002: Interannual variability in the tropical Indian Ocean. *J. Geophys. Res.*, **107**, 3199, <https://doi.org/10.1029/2001JC001278>.

Hurrell, J. W., and Coauthors, 2013: The Community Earth System Model: A framework for collaborative research. *Bull. Amer. Meteor. Soc.*, **94**, 1339–1360, <https://doi.org/10.1175/BAMS-D-12-00121.1>.

Izumo, T., and Coauthors, 2010: Influence of the state of the Indian Ocean dipole on the following years El Niño. *Nat. Geosci.*, **3**, 168–172, <https://doi.org/10.1038/ngeo760>.

—, J. Vialard, M. Lengaigne, and I. Suresh, 2020: Relevance of relative sea surface temperature for tropical rainfall interannual variability. *Geophys. Res. Lett.*, **47**, e2019GL086182, <https://doi.org/10.1029/2019GL086182>.

Jourdain, N. C., M. Lengaigne, J. Vialard, T. Izumo, and A. Sen Gupta, 2016: Further insights on the influence of the Indian Ocean dipole on the following year's ENSO from observations and CMIP5 models. *J. Climate*, **29**, 637–658, <https://doi.org/10.1175/JCLI-D-15-0481.1>.

Kataoka, T., T. Tozuka, S. Behera, and T. Yamagata, 2014: On the Ningaloo Niño/Niña. *Climate Dyn.*, **43**, 1463–1482, <https://doi.org/10.1007/s00382-013-1961-z>.

Kay, J. E., and Coauthors, 2015: The Community Earth System Model (CESM) large ensemble project: A community resource for studying climate change in the presence of internal climate variability. *Bull. Amer. Meteor. Soc.*, **96**, 1333–1349, <https://doi.org/10.1175/BAMS-D-13-00255.1>.

Klein, S. A., B. J. Soden, and N.-C. Lau, 1999: Remote sea surface temperature variations during ENSO: Evidence for a tropical atmospheric bridge. *J. Climate*, **12**, 917–932, [https://doi.org/10.1175/1520-0442\(1999\)012<0917:RSSTVD>2.0.CO;2](https://doi.org/10.1175/1520-0442(1999)012<0917:RSSTVD>2.0.CO;2).

Kosaka, Y., and S. P. Xie, 2013: Recent global-warming hiatus tied to equatorial Pacific surface cooling. *Nature*, **501**, 403–407, <https://doi.org/10.1038/nature12534>.

Krishnamurthy, V., and B. P. Kirtman, 2003: Variability of the Indian Ocean: Relation to monsoon and ENSO. *Quart. J. Roy. Meteor. Soc.*, **129**, 1623–1646, <https://doi.org/10.1256/qj.01.166>.

Li, Y., W. Han, T. Shinoda, C. Wang, M. Ravichandran, and J.-W. Wang, 2014: Revisiting the wintertime intraseasonal SST variability in the tropical South Indian Ocean: Impact of the ocean interannual variation. *J. Phys. Oceanogr.*, **44**, 1886–1907, <https://doi.org/10.1175/JPO-D-13-0238.1>.

Luo, J. J., R. Zhang, S. K. Behera, Y. Masumoto, F. F. Jin, R. Lukas, and T. Yamagata, 2010: Interaction between El Niño and extreme Indian Ocean dipole. *J. Climate*, **23**, 726–742, <https://doi.org/10.1175/2009JCLI3104.1>.

Marshall, A. G., H. H. Hendon, M. Feng, and A. Schiller, 2015: Initiation and amplification of the Ningaloo Niño. *Climate Dyn.*, **45**, 2367–2385, <https://doi.org/10.1007/s00382-015-2477-5>.

McCreary, J. P., P. K. Kundu, and R. L. Molinari, 1993: A numerical investigation of dynamics, thermodynamics and mixed-layer processes in the Indian Ocean. *Prog. Oceanogr.*, **31**, 181–244, [https://doi.org/10.1016/0079-6611\(93\)90002-U](https://doi.org/10.1016/0079-6611(93)90002-U).

McPhaden, M. J., and M. Nagura, 2014: Indian Ocean dipole interpreted in terms of recharge oscillator theory. *Climate Dyn.*, **42**, 1569–1586, <https://doi.org/10.1007/s00382-013-1765-1>.

—, S. E. Zebiak, and M. H. Glantz, 2006: ENSO as an integrating concept in Earth science. *Science*, **314**, 1740–1745, <https://doi.org/10.1126/science.1132588>.

Meehl, G. A., 1997: The South Asian monsoon and the tropospheric biennial oscillation. *J. Climate*, **10**, 1921–1943, [https://doi.org/10.1175/1520-0442\(1997\)010<1921:TSAMAT>2.0.CO;2](https://doi.org/10.1175/1520-0442(1997)010<1921:TSAMAT>2.0.CO;2).

—, and J. M. Arblaster, 2002: The tropospheric biennial oscillation and Asian–Australian monsoon rainfall. *J. Climate*, **15**, 722–744, [https://doi.org/10.1175/1520-0442\(2002\)015<0722:TTBOAA>2.0.CO;2](https://doi.org/10.1175/1520-0442(2002)015<0722:TTBOAA>2.0.CO;2).

Meyers, G., P. McIntosh, L. Pigot, and M. Pook, 2007: The years of El Niño, La Niña, and interactions with the tropical Indian Ocean. *J. Climate*, **20**, 2872–2880, <https://doi.org/10.1175/JCLI4152.1>.

Morioka, Y., T. Tozuka, S. Masson, P. Terray, J. J. Luo, and T. Yamagata, 2012: Subtropical dipole modes simulated in a coupled general circulation model. *J. Climate*, **25**, 4029–4047, <https://doi.org/10.1175/JCLI-D-11-00396.1>.

Murtugudde, R., and A. J. Busalacchi, 1999: Interannual variability of the dynamics and thermodynamics of the tropical Indian Ocean. *J. Climate*, **12**, 2300–2326, [https://doi.org/10.1175/1520-0442\(1999\)012<2300:IVOTDA>2.0.CO;2](https://doi.org/10.1175/1520-0442(1999)012<2300:IVOTDA>2.0.CO;2).

Ohba, M., and H. Ueda, 2007: An impact of SST anomalies in the Indian Ocean in acceleration of the El Niño to La Niña

transition. *J. Meteor. Soc. Japan*, **85**, 335–348, <https://doi.org/10.2151/jmsj.85.335>.

Poli, P., and Coauthors, 2016: ERA-20C: An atmospheric reanalysis of the twentieth century. *J. Climate*, **29**, 4083–4097, <https://doi.org/10.1175/JCLI-D-15-0556.1>.

Rao, S. A., and T. Yamagata, 2004: Abrupt termination of Indian Ocean dipole events in response to intraseasonal disturbances. *Geophys. Res. Lett.*, **31**, L19306, <https://doi.org/10.1029/2004GL020842>.

—, —, and S. K. Behera, 2005: Subsurface influence on SST in the tropical Indian Ocean: Structure and interannual variability. *Dyn. Atmos. Oceans*, **39**, 103–135, <https://doi.org/10.1016/j.dynatmoc.2004.10.014>.

—, —, Y. Masumoto, and T. Yamagata, 2002: Interannual subsurface variability in the tropical Indian Ocean with a special emphasis on the Indian Ocean dipole. *Deep-Sea Res. II*, **49**, 1549–1572, [https://doi.org/10.1016/S0967-0645\(01\)00158-8](https://doi.org/10.1016/S0967-0645(01)00158-8).

Rayner, N. A., D. E. Parker, E. B. Horton, C. K. Folland, L. V. Alexander, D. P. Rowell, E. C. Kent, and A. Kaplan, 2003: Global analyses of sea surface temperature, sea ice, and night marine air temperature since the late nineteenth century. *J. Geophys. Res.*, **108**, 4407, <https://doi.org/10.1029/2002JD002670>.

Saji, N. H., and T. Yamagata, 2003: Possible impacts of Indian Ocean dipole mode events on global climate. *Climate Res.*, **25**, 151–169, <https://doi.org/10.3354/cr025151>.

—, B. N. Goswami, P. N. Vinayachandran, and T. Yamagata, 1999: A dipole mode in the tropical Indian Ocean. *Nature*, **401**, 360–363, <https://doi.org/10.1038/43854>.

Shinoda, T., M. A. Alexander, and H. H. Hendon, 2004: Remote response of the Indian Ocean to interannual SST variations in the tropical Pacific. *J. Climate*, **17**, 362–372, [https://doi.org/10.1175/1520-0442\(2004\)017<0362:RROTIO>2.0.CO;2](https://doi.org/10.1175/1520-0442(2004)017<0362:RROTIO>2.0.CO;2).

Smith, T. M., R. W. Reynolds, T. C. Peterson, and J. Lawrimore, 2008: Improvements to NOAA's historical merged land-ocean surface temperature analysis (1880–2006). *J. Climate*, **21**, 2283–2296, <https://doi.org/10.1175/2007JCLI2100.1>.

Stuecker, M. F., A. Timmermann, F. F. Jin, Y. Chikamoto, W. Zhang, A. T. Wittenberg, E. Widiasih, and S. Zhao, 2017: Revisiting ENSO/Indian Ocean dipole phase relationships. *Geophys. Res. Lett.*, **44**, 2481–2492, <https://doi.org/10.1002/2016GL072308>.

Terray, P., and S. Dominik, 2005: Indian Ocean sea surface temperature and El Niño–Southern Oscillation: A new perspective. *J. Climate*, **18**, 1351–1368, <https://doi.org/10.1175/JCLI3338.1>.

—, S. Masson, C. Prodhomme, M. K. Roxy, and K. P. Sooraj, 2016: Impacts of Indian and Atlantic Oceans on ENSO in a comprehensive modeling framework. *Climate Dyn.*, **46**, 2507–2533, <https://doi.org/10.1007/s00382-015-2715-x>.

Tozuka, T., T. Kataoka, and T. Yamagata, 2014: Locally and remotely forced atmospheric circulation anomalies of Ningaloo Niño/Niña. *Climate Dyn.*, **43**, 2197–2205, <https://doi.org/10.1007/s00382-013-2044-x>.

Wallace, J. M., and D. S. Gutzler, 1981: Teleconnections in the geopotential height field during the Northern Hemisphere winter. *Mon. Wea. Rev.*, **109**, 784–812, [https://doi.org/10.1175/1520-0493\(1981\)109<0784:TITGHF>2.0.CO;2](https://doi.org/10.1175/1520-0493(1981)109<0784:TITGHF>2.0.CO;2).

Webster, P. J., A. M. Moore, J. P. Loschnigg, and R. R. Leben, 1999: Coupled ocean–atmosphere dynamics in the Indian Ocean during 1997–98. *Nature*, **401**, 356–360, <https://doi.org/10.1038/43848>.

Weller, E., and W. Cai, 2013: Realism of the Indian Ocean dipole in CMIP5 models: The implications for climate projections. *J. Climate*, **26**, 6649–6659, <https://doi.org/10.1175/JCLI-D-12-00807.1>.

Wieners, C. E., H. A. Dijkstra, and W. P. M. de Ruijter, 2017: The influence of atmospheric convection on the interaction between the Indian Ocean and ENSO. *J. Climate*, **30**, 10 155–10 178, <https://doi.org/10.1175/JCLI-D-17-0081.1>.

—, —, and —, 2019: The interaction between the western Indian Ocean and ENSO in CESM. *Climate Dyn.*, **52**, 5153–5172, <https://doi.org/10.1007/s00382-018-4438-2>.

Xie, S.-P., and S. G. H. Philander, 1994: A coupled ocean–atmosphere model of relevance to the ITCZ in the eastern Pacific. *Tellus*, **46A**, 340–350, <https://doi.org/10.3402/tellusa.v46i4.15484>.

—, H. Annamalai, F. A. Schott, and J. P. McCreary, 2002: Structure and mechanisms of south Indian Ocean climate variability. *J. Climate*, **15**, 864–878, [https://doi.org/10.1175/1520-0442\(2002\)015<0864:SAMOSI>2.0.CO;2](https://doi.org/10.1175/1520-0442(2002)015<0864:SAMOSI>2.0.CO;2).

Yang, Y., S. P. Xie, L. Wu, Y. Kosaka, N.-C. Lau, and G. A. Vecchi, 2015: Seasonality and predictability of the Indian Ocean dipole mode: ENSO forcing and internal variability. *J. Climate*, **28**, 8021–8036, <https://doi.org/10.1175/JCLI-D-15-0078.1>.

—, J. Li, L. Wu, Y. Kosaka, Y. Du, C. Sun, F. Xie, and J. Feng, 2017: Decadal Indian Ocean dipolar variability and its relationship with the tropical Pacific. *Adv. Atmos. Sci.*, **34**, 1282–1289, <https://doi.org/10.1007/s00376-017-7009-2>.

Yokoi, T., T. Tozuka, and T. Yamagata, 2008: Seasonal variation of the Seychelles Dome. *J. Climate*, **21**, 3740–3754, <https://doi.org/10.1175/2008JCLI1957.1>.

Zhang, H., A. Clement, P. Di Nezio, H. Zhang, A. Clement, and P. Di Nezio, 2014: The South Pacific meridional mode: A mechanism for ENSO-like variability. *J. Climate*, **27**, 769–783, <https://doi.org/10.1175/JCLI-D-13-00082.1>.

Zhang, L., and W. Han, 2018: Impact of Ningaloo Niño on tropical Pacific and an interbasin coupling mechanism. *Geophys. Res. Lett.*, **45**, 11 300–11 309, <https://doi.org/10.1029/2018GL078579>.

—, —, and —, 2020: Barrier for the eastward propagation of Madden–Julian Oscillation over the Maritime Continent: A possible new mechanism. *Geophys. Res. Lett.*, **47**, e2020GL090211, <https://doi.org/10.1029/2020GL090211>.

—, —, Y. Li, and T. Shinoda, 2018: Mechanisms for generation and development of the Ningaloo Niño. *J. Climate*, **31**, 9239–9259, <https://doi.org/10.1175/JCLI-D-18-0175.1>.

—, —, K. B. Karnauskas, G. A. Meehl, A. Hu, N. Rosenbloom, and T. Shinoda, 2019: Indian Ocean warming trend reduces Pacific warming response to anthropogenic greenhouse gases: An interbasin thermostat mechanism. *Geophys. Res. Lett.*, **46**, 10 882–10 890, <https://doi.org/10.1029/2019GL084088>.

—, —, and Z.-Z. Hu, 2021a: Inter-basin and multi-time scale interactions in generating the 2019 extreme Indian Ocean dipole. *J. Climate*, **34**, 4553–4566, <https://doi.org/10.1175/JCLI-D-20-0760.1>.

—, —, G. Wang, M. Newman, and W. Han, 2021b: Interannual to decadal variability of tropical Indian Ocean sea surface temperature: Pacific influence versus local internal variability. *J. Climate*, **34**, 2669–2684, <https://doi.org/10.1175/JCLI-D-20-0807.1>.

Zhang, W., Y. Wang, F.-F. Jin, M. F. Stuecker, and A. G. Turner, 2015: Impact of different El Niño types on the El Niño/IOD relationship. *Geophys. Res. Lett.*, **42**, 8570–8576, <https://doi.org/10.1002/2015GL065703>.

Zhao, S., F.-F. Jin, and M. F. Stuecker, 2019: Improved predictability of the Indian Ocean dipole using seasonally modulated ENSO forcing forecasts. *Geophys. Res. Lett.*, **46**, 9980–9990, <https://doi.org/10.1029/2019GL084196>.

—, M. F. Stuecker, F.-F. Jin, J. Feng, H.-L. Ren, W. Zhang, and J. Li, 2020: Improved predictability of the Indian Ocean dipole using a stochastic dynamical model compared to the North American Multimodel Ensemble forecast. *Wea. Forecasting*, **35**, 379–399, <https://doi.org/10.1175/WAF-D-19-0184.1>.